

Supporting information

The Rate-Limiting Step in the Batteries with Metal Oxides as the Energy Materials

Qiang Wang[†], *Mingchao Shang*[†], *Yong Zhang*[‡], *Yuan Yang*[§], *Yan Wang*^{*†}

[†] Materials Science & Engineering, Worcester Polytechnic Institute, 100 Institute Road, Worcester, MA 01609;

[‡] Center for Materials Science and Engineering, Massachusetts Institute of Technology, 77 Massachusetts Ave., Cambridge, MA 02139;

[§] Materials Science & Engineering, Columbia University, 200 S.W. Mudd, New York, NY 10027.

Keywords: metal oxides, O²⁻ ions diffusion, rate-limiting step, diffusion coefficient, defects.

1. Reproducibility of CV testing for Fe₂O₃ ink electrode.

α -Fe₂O₃ ink electrode (200 nm) is inserted into four-neck flask for CV testing, and three CV profiles and peak current density, which came from three similar ink electrodes, are shown in Fig. S 1 and Table S1. The relative deviation is under 4%, which demonstrates that the results have a good reproducibility, and the ink electrode is a reliable tool for the analysis of electrode process dynamics.

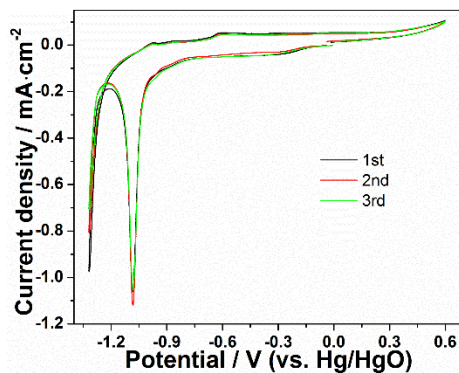


Fig. S1. Three CV tests about Fe₂O₃ (200 nm) ink electrode in alkaline electrolyte (20wt% KOH solution).

Table S1. The peak currents density of the three CV tests and their relative deviation.

Number of electrodes	Reduction peak current density of Fe ³⁺ to Fe ²⁺ (i_p (Fe ³⁺ to Fe ²⁺))	Relative deviation of current density
1	-1.053 mA·cm ⁻²	2.2%
2	-1.058 mA·cm ⁻²	1.7%
3	-1.120 mA·cm ⁻²	3.9%

2. The CV test of the α -Fe₂O₃ (40 nm) ink electrodes

The morphology of α -Fe₂O₃ (40 nm) particles on glass carbon was analyzed by SEM, as shown in Fig. S2. Several α -Fe₂O₃ (40 nm) ink electrodes were prepared, and each ink electrode was just scanned once at one scan rate, because when the same α -Fe₂O₃ (40nm) ink

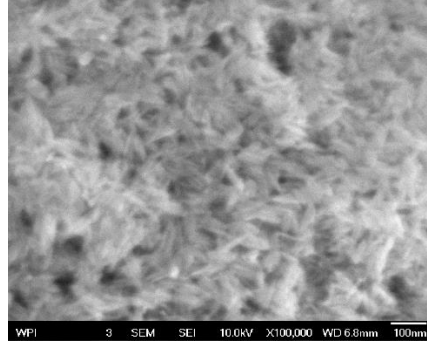


Fig. S2. The morphology of α -Fe₂O₃ (40 nm) particles analyzed by SEM.

electrode is scanned for the second time, Fe(OH)₃ and Fe(OH)₂ co-exist with α -Fe₂O₃. Fig. S 3 shows CV profiles at a series of scan rates. The width of the cathodic peak increased gradually with scan rate increasing, and a shoulder peak appeared with the scan rate larger than 10 mV·s⁻¹.

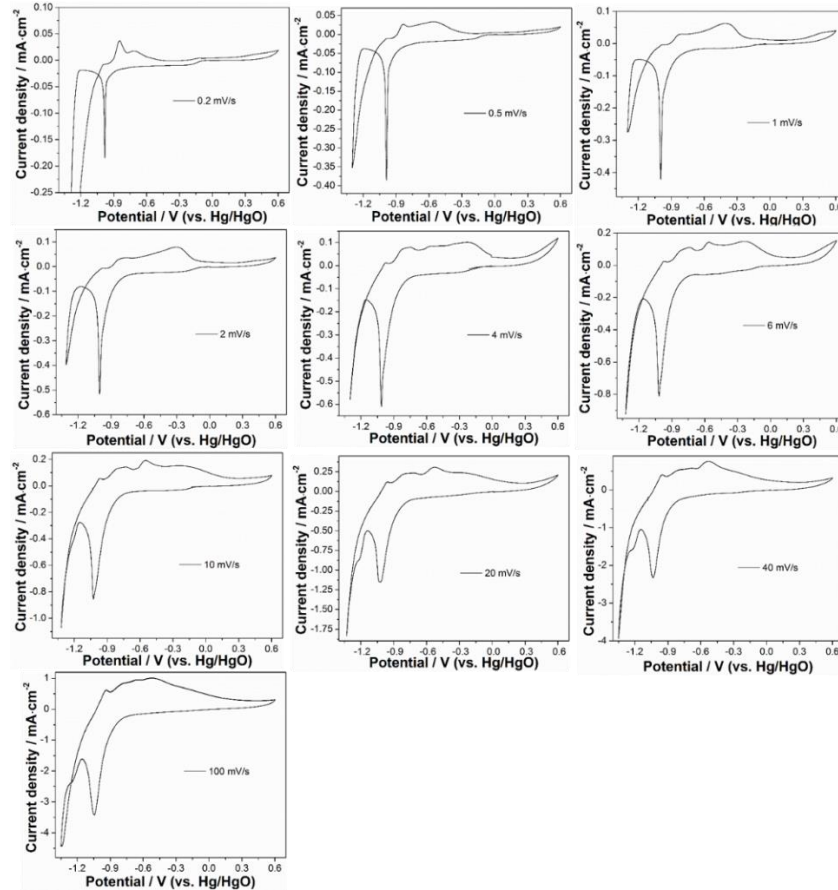


Fig. S3. The CV profiles of the α -Fe₂O₃ (40nm) ink electrodes in 20 wt% KOH solution with a series of scan rates from 0.2 mV/s to 100 mV/s.

To investigate the relationship between current density of the cathodic peak and the scan rate, the background current density was subtracted from the peak current density, and the operation was shown in Fig. S4. The cathodic peak current density in all the CV profiles of this manuscript was calibrated in the same way, thus the current density occurred from EDL capacitance, residue O₂ reduction and formation of amorphous Fe(OH)₂ shell was subtracted from the peak current density.

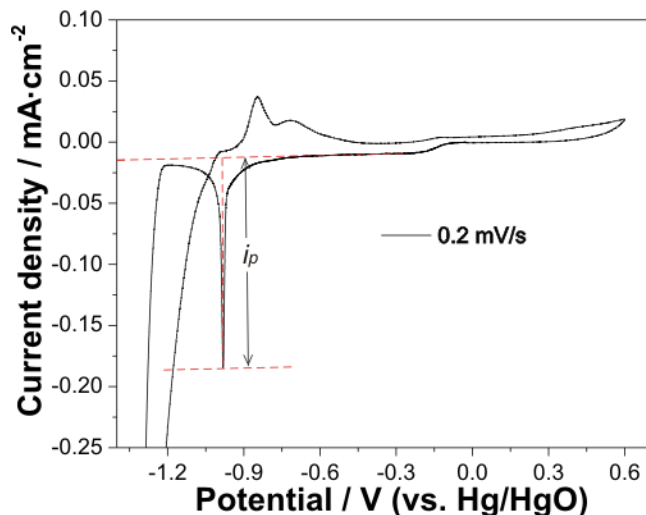


Fig. S4. The calibration of the current density of cathodic peak.

The calibrated peak current density in the CV profile at different scan rates was shown in Table S2.

Table S2. The calculated peak current density in the CV profiles of α -Fe₂O₃ (40 nm) with different scan rate.

Scan rate / mV · s ⁻¹	Calculated peak current density / mA·cm ²
0.2	-0.171
0.5	-0.357
1	-0.396
2	-0.483
4	-0.559
6	-0.739
10	-0.800
20	-1.027
40	-2.122
100	-3.203

3. The CV test of the α -Fe₂O₃ (200 nm) ink electrodes

The morphology of α -Fe₂O₃ (200 nm) particles on glass carbon was analyzed with SEM, as shown in Fig. S5. Several α -Fe₂O₃ (200 nm) ink electrodes were prepared, and each

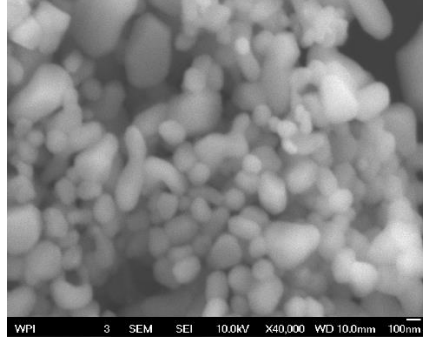


Fig. S5. The morphology of α -Fe₂O₃ (200 nm) particles analyzed by SEM.

ink electrode was just scanned once at one scan rate. Fig. S6 shows CV profiles at a series of scan rate. The width of the cathodic peak also increased gradually with scan rate increasing.

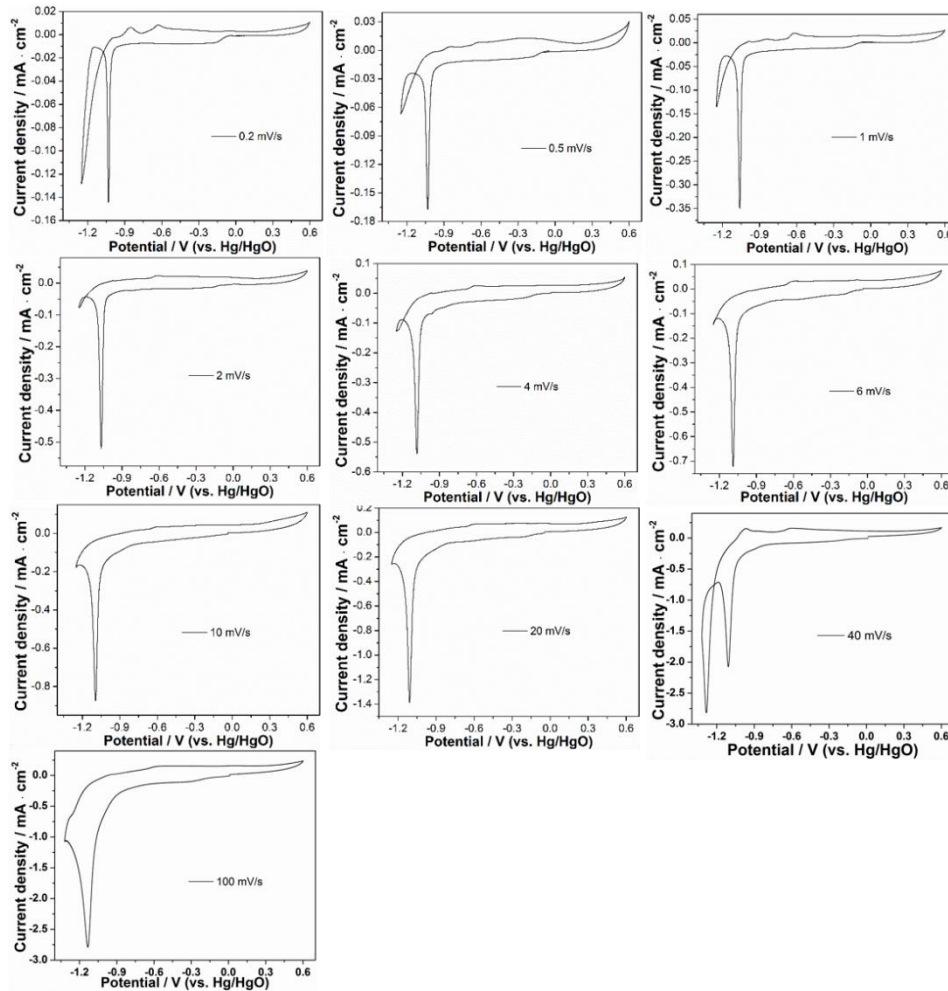


Fig. S6. The CV profiles of the α -Fe₂O₃ (200 nm) ink electrodes in 20 wt% KOH solution with a series of scan rates from 0.2 mV/s to 100 mV/s.

The calibrated peak current density in the CV profile at different scan rates was shown in Table S3.

Table S3. The calculated peak current density in the CV profiles of α -Fe₂O₃ (200 nm) with different scan rate.

Scan rate / mV · s ⁻¹	Calculated peak current density / mA·cm ²
0.2	-0.171
0.5	-0.357
1	-0.396
2	-0.483
4	-0.559
6	-0.739
10	-0.800
20	-1.027
40	-2.122
100	-3.203

4. The characterization of hexagonal flake crystal by TEM and electron diffraction pattern

The overall appearance of the hexagonal flake is shown in Fig. S7 (a), and Fig. S7 (b) shows the crystal lattice inside the flake. The flake was indexed as $\text{Fe}(\text{OH})_2$ type hexagonal crystal structure ($a = 0.3262 \text{ nm}$, $c = 0.4596 \text{ nm}$) by SAED pattern.

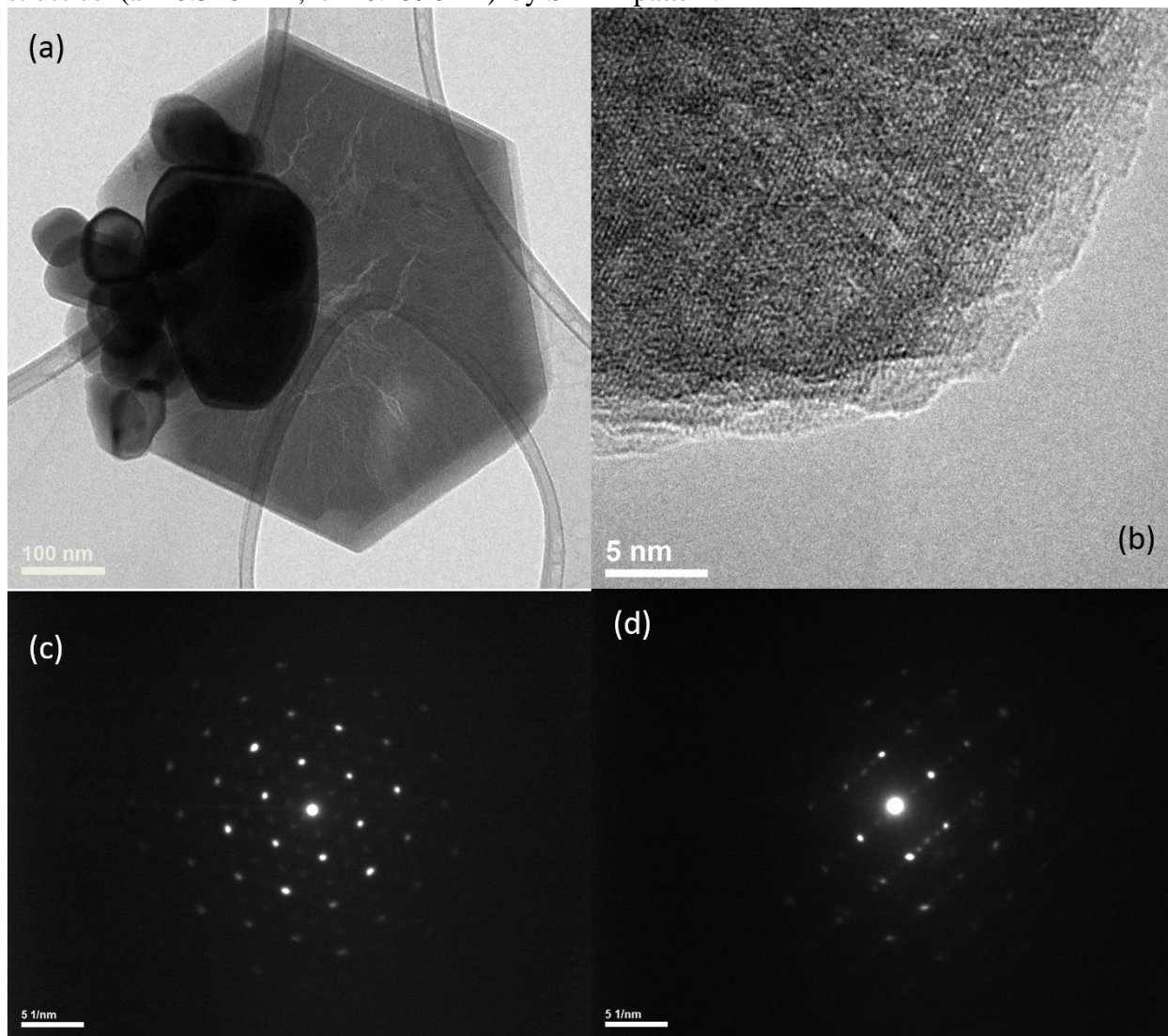


Fig. S7. TEM and electron diffraction analysis of the hexagonal flake. (a) Overall morphology of the hexagonal flake; (b) crystal lattice image inside the flake; (c) and (d) SAED (selected Area Electron Diffraction) patterns at [001] and [111] directions respectively.

5. TEM analysis of the integral Fe_2O_3 particles scanned to different potentials

In order to reveal the crystal lattice and defect inside Fe_2O_3 particles, TEM just focused on a part of the particles in Fig. 3. The entire particles corresponding to Fig. 3 are shown in Fig. S8.

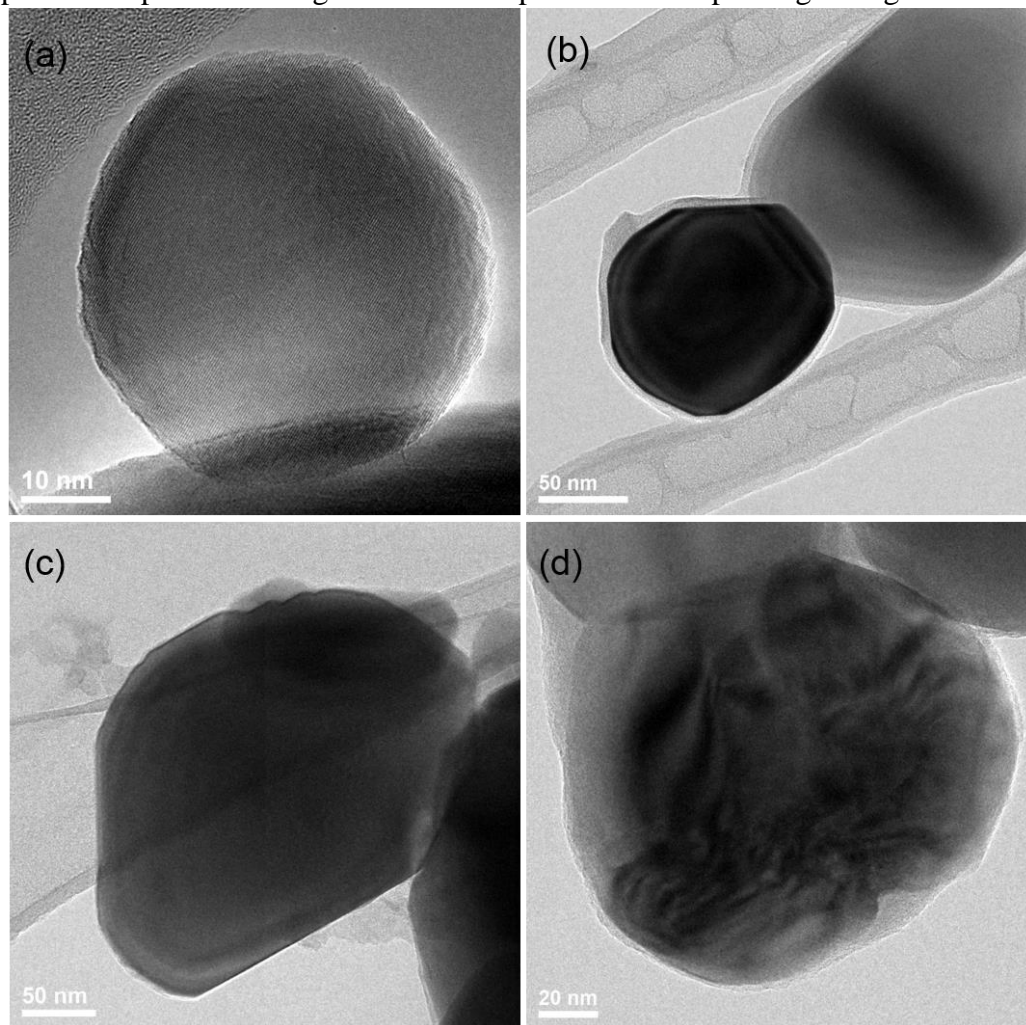


Fig. S8. The entire $\alpha\text{-Fe}_2\text{O}_3$ particles scanned to different potential. (a) The particle before LSV test; (b) the particle scanned to -0.9 V (vs. Hg/HgO); (c) the particle scanned to -1.012 V (vs. Hg/HgO); and (d) the particle scanned to -1.2 V (vs. Hg/HgO).

6. TEM analysis of the Fe_2O_3 particles scanned to -0.9 V at two scan rates

Two Fe_2O_3 ink electrodes were scanned from OCV to -0.9 V at the scan rate of 1 mV/s and 0.1 mV/s separately, and the particles from these two electrode were analyzed by TEM individually, as shown in Fig. S9. At higher scan rate, the thickness of the amorphous shell is thinner.

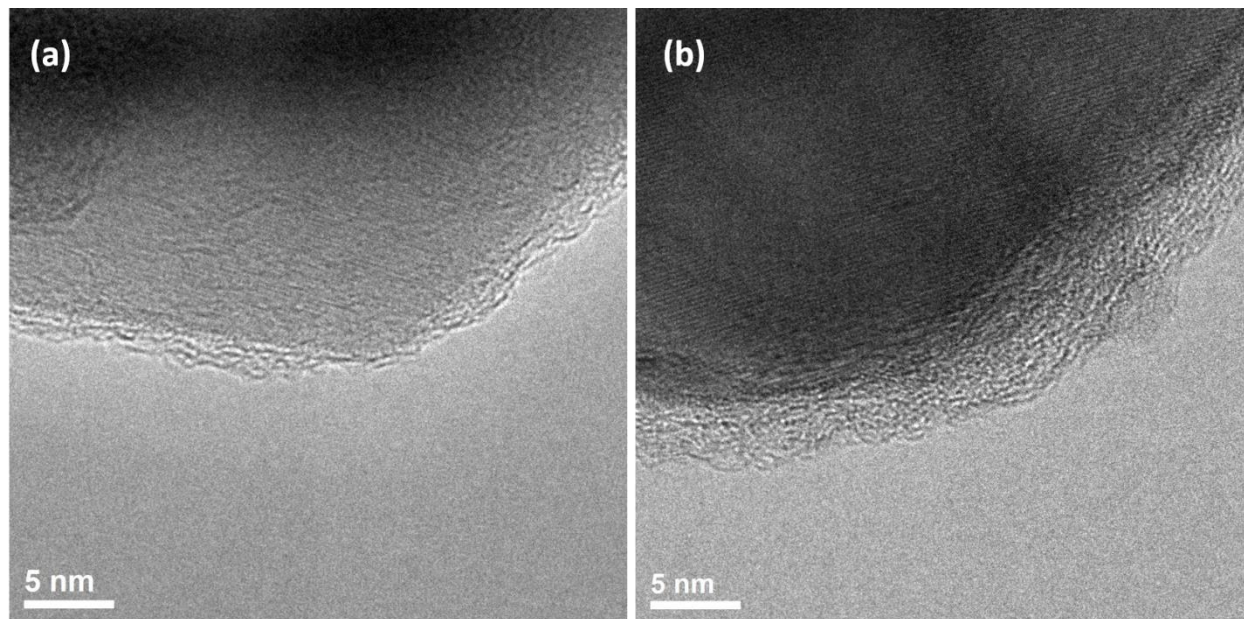


Fig. S9. TEM analysis of Fe_2O_3 particles (200 nm) scanned to -0.9 V at the scan rate of 1 mV/s and 0.1 mV/s separately. (a) Fe_2O_3 particle scanned to -0.9 V at 1 mV/s; (b) Fe_2O_3 particle scanned to -0.9 V at 0.1 mV/s

7. SEM characterization of CuO particles and CV test of CuO ink electrodes

The morphology of CuO particles on glass carbon was analyzed by SEM, as shown in Fig. S10, and CuO ink electrodes were prepared by using the particles. Each electrode was just tested

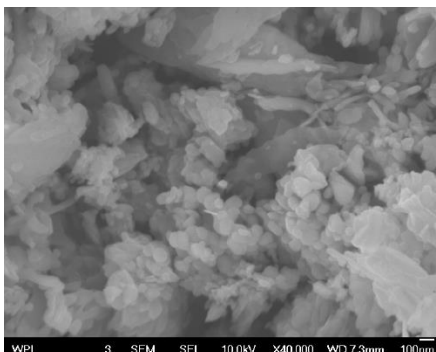


Fig. S10. The morphology of CuO particle.

once at a scan rate, and their CV profiles are shown in Fig. S11. One cathodic peak appears at low scan rate of 1 mV/s, but the peak splitted into two cathodic peaks, when the scan rate increased.

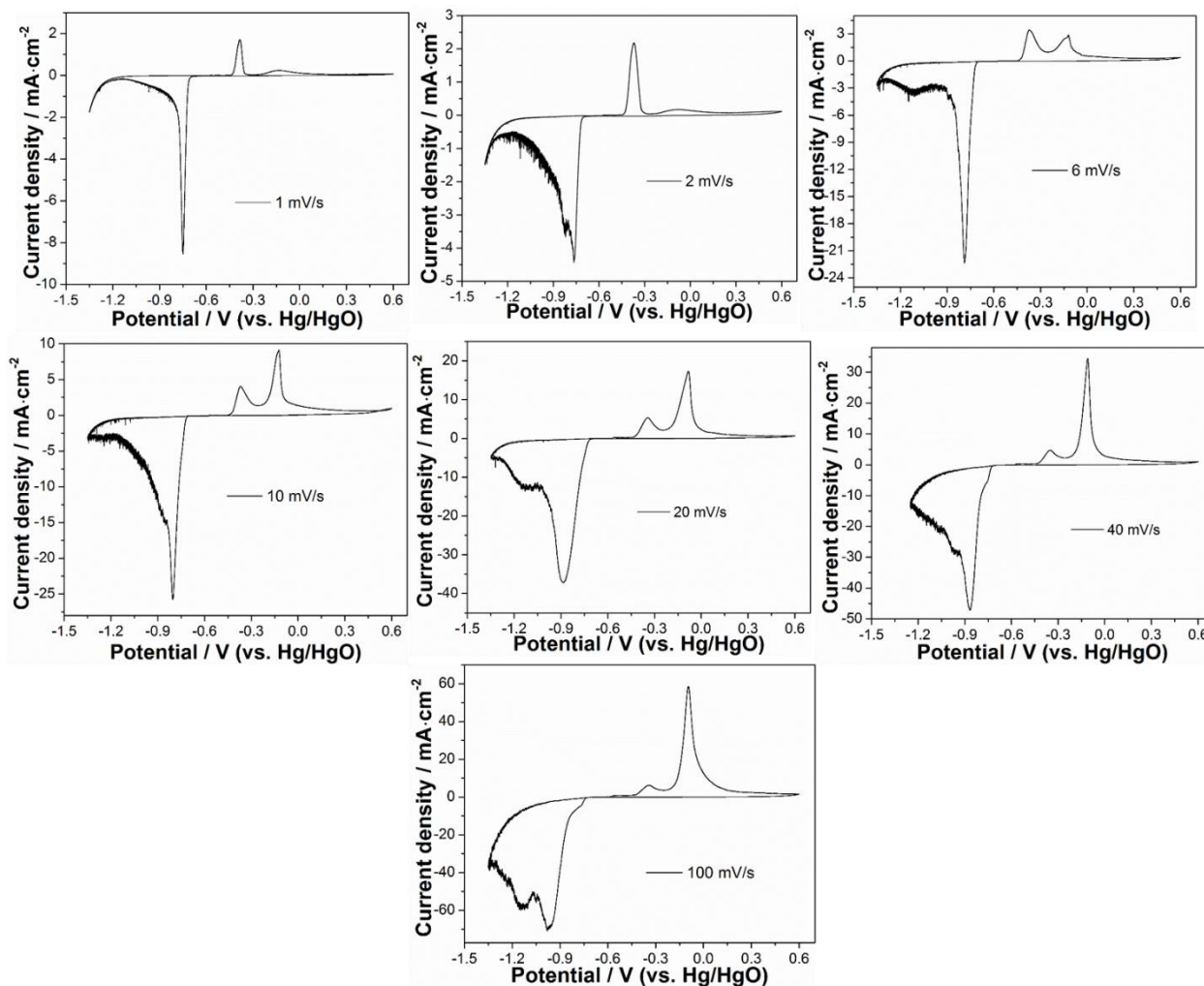


Fig. S11. The CV profiles of the CuO ink electrodes in 20 wt% KOH solution with a series of scan rates from 1 mV/s to 100 mV/s.

Table S4. The calculated peak current density in the CV profiles of CuO ink electrodes with different scan rates.

Scan rate (mV·s ⁻¹)	Peak current density (mA/cm ²)
1	-8.543
2	-4.429
6	-22.357
10	-25.685
20	-37.21
40	-47.161
100	-70.417

The CuO particle scanned to the peak potential of -0.75 V (vs. Hg/HgO) was analyzed with TEM. Fig. S12 shows that the particle has defects inside the bulk, and the surface of the particle is still crystal structure as the arrows pointed.

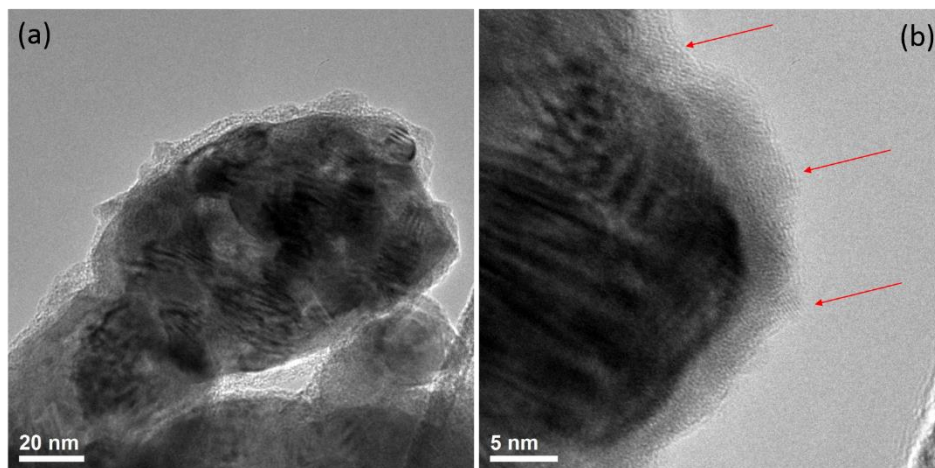


Fig. S12. The CuO particle scanned to the peak potential of -0.75 V (vs. Hg/HgO). (a) The entire CuO particle; (b) a part of CuO particle with crystal surface as the arrows pointed, and defects inside the crystal matrix.

8. The CV profiles of the Bi_2O_3 (40nm) ink electrodes.

The morphology of Bi_2O_3 particles on glass carbon was analyzed with SEM, as shown in Fig. S13, and Bi_2O_3 ink electrodes were prepared by using the particles. Each electrode was just tested

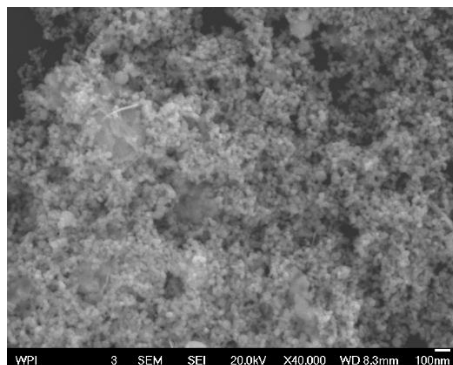


Fig. S13. The morphology of Bi_2O_3 particle.

once at a scan rate, and their CV profiles was shown in Fig. S14.

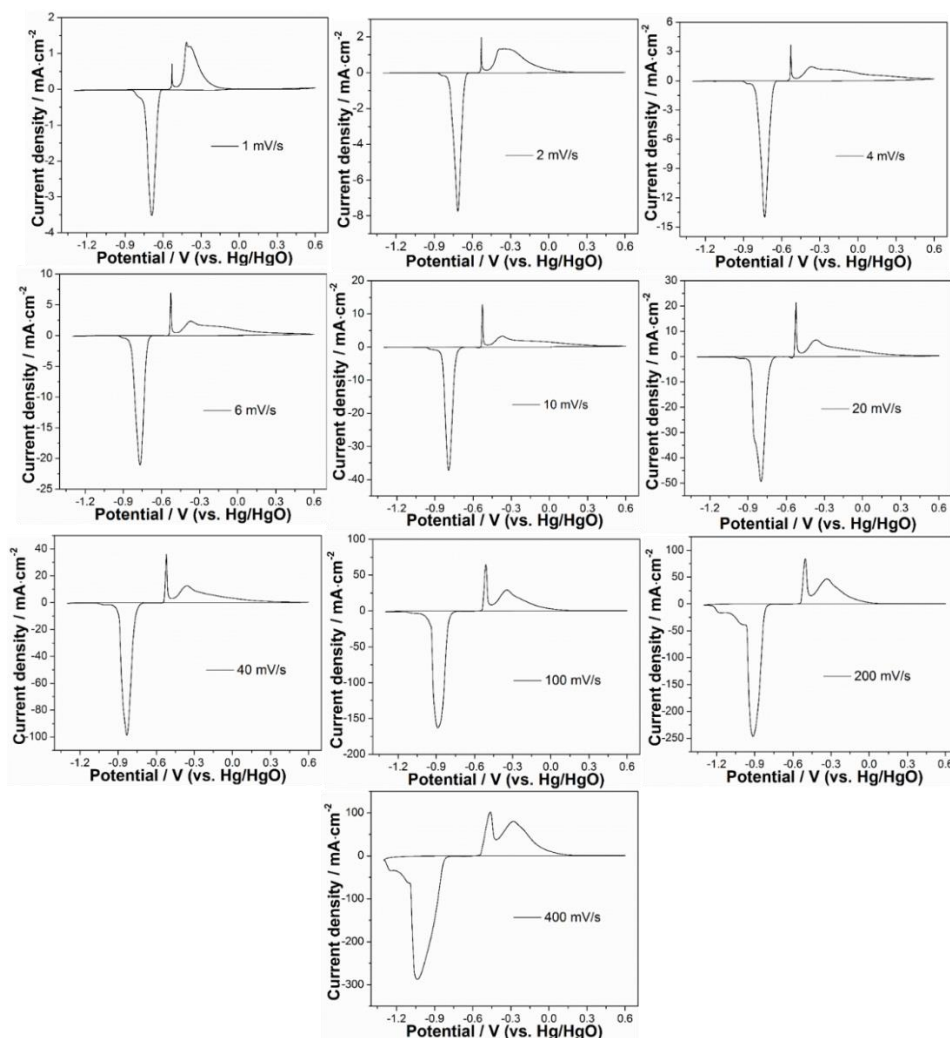


Fig. S14. the CV profiles of the Bi_2O_3 ink electrodes in 20 wt% KOH solution with a series of scan rates from 1 mV/s to 400 mV/s.

Table S5. The peak current density in the CV profile of Bi_2O_3 ink electrodes with different scan rates.

Scan rate (mV/s)	Peak current density (mA/cm ²)
1	-0.144
2	-0.167
4	-0.350
6	-0.520
10	-0.540
20	-0.721
40	-0.874
100	-1.387
200	-2.075
400	-2.789

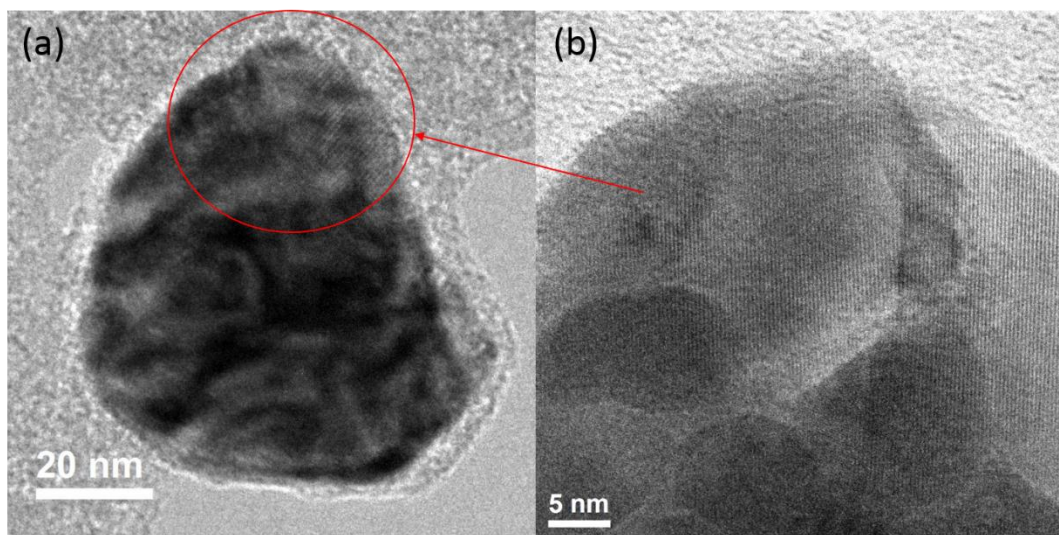


Fig. S15. TEM analysis of Bi_2O_3 particle, which was scanned to the peak potential of -0.7 V (vs. Hg/HgO). (a) TEM analysis of the integral Bi_2O_3 particle; (b) high resolution TEM image of the particle, which shows the surface of the particle is crystal structure.

9. SEM characterization of Fe₃O₄ particle and CV test of Fe₃O₄ ink electrodes

The morphology of Fe₃O₄ particle on glass carbon was analyzed with SEM, as shown in Fig. S16, and each electrode was just tested once at a scan rate. Their CV profiles are shown in Fig. S17. Two cathodic peaks appears in the CV profile, which were marked as peak i and ii in Fig. S17. According to the experiment of α -Fe₂O₃ reduction, peak i was due to both reaction pathways

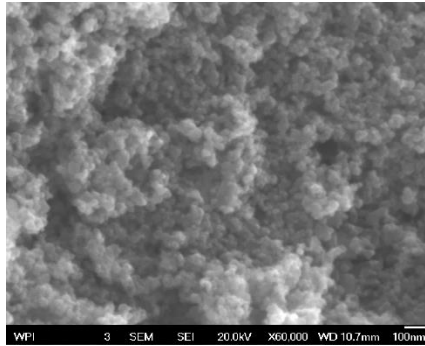


Fig. S16. The morphology of Fe₃O₄ particle analyzed by SEM.

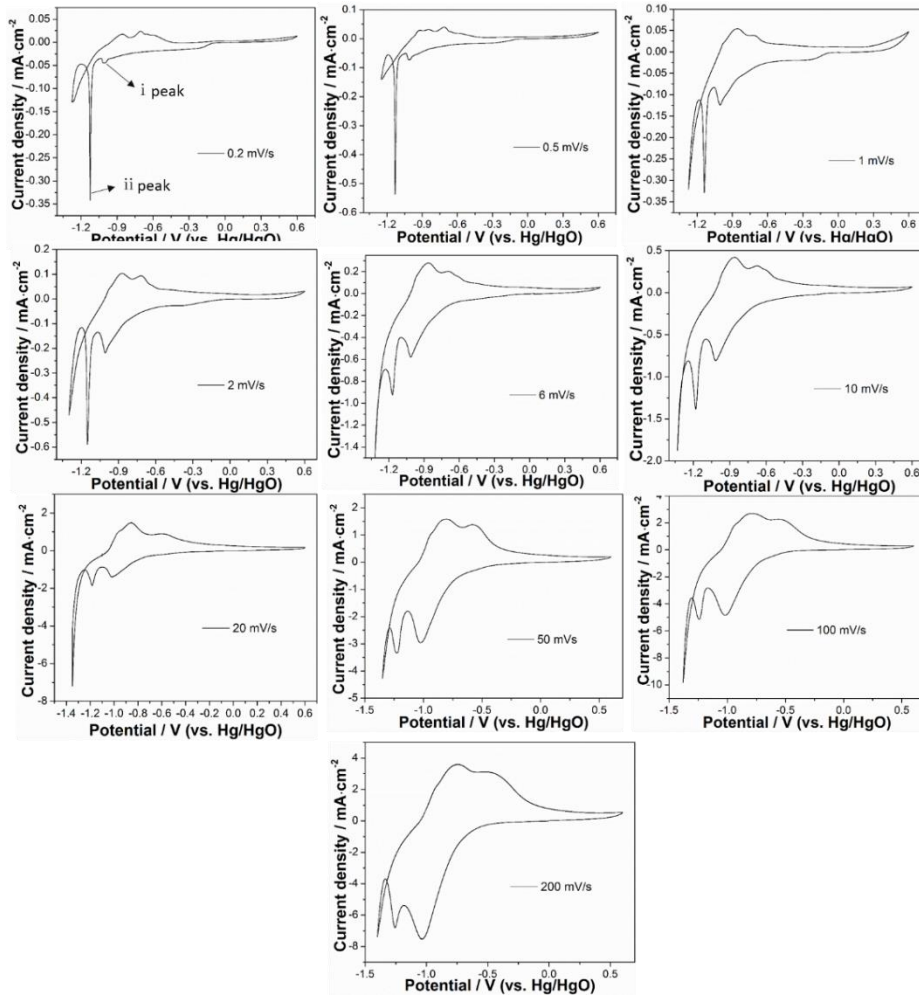


Fig. S17. The CV profiles of the Fe₃O₄ ink electrodes in 20 wt% KOH solution with a series of scan rates from 0.2 mV/s to 200 mV/s.

of forming Fe(OH)_{2/amor} outside and O²⁻ defects inside particles. Peak ii was mainly attributed to the continuous formation of O²⁻ defects. The peak current density was estimated in the same way as Fig. S4 shown, and the relationship between these two peaks current density and scan rate was determined. The result was very interesting, as in the scan rate range from 0.2 mV/s to 6 mV/s, the current density of peak i was strictly proportional to the scan rate, as shown in Fig. S18 (a). The data points fitted with the fitting line very well with the adjusted R² of 0.999. In the scan rate range from 10 mV/s to 200 mV/s, the current density of peak i was obviously not proportional to scan rate, but can barely be proportional to the square root of scan rate, as shown in Fig. S18 (b). However, the current density of peak ii was always proportional to square root of the scan rate from 0.2 mV/s to 200 mV/s, as shown in Fig. S18 (c). The peak current density and the scan rate relationship demonstrates ions diffusion inside the crystal matrix of Fe₃O₄ is the rate-limiting step.

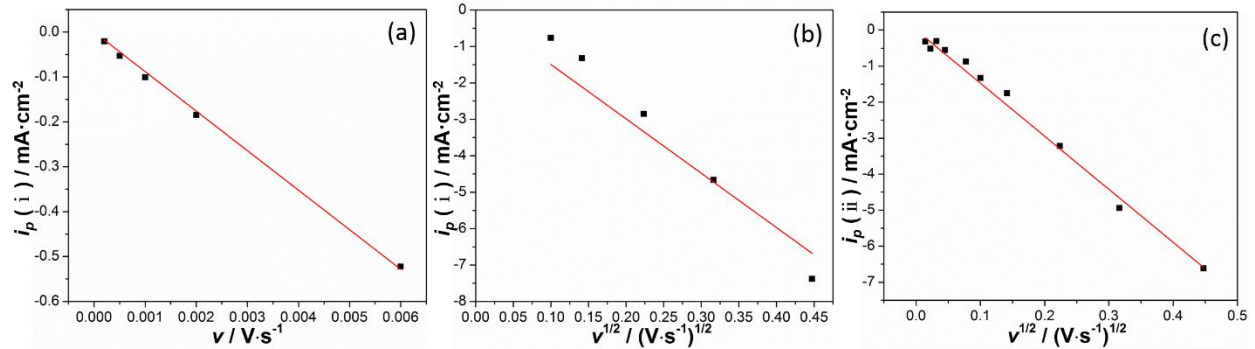


Fig. S18. The relationship between current density of peak i and ii and scan rate. (a) the current density of peak i is proportionate to scan rate, when scan rate was no larger than 6 mV/s; (b) the current density tend to be proportionate to square root of scan rate, when scan rate was larger than 6 mV/s; (c) the current density of peak ii was proportionate of square root to scan rate in a wide range.

Large size of Fe₃O₄ particles (~100 nm) were scanned from OCP to -1.132 V (vs. Hg/HgO) (peak i), because relatively large particles can be more easily tracked by TEM and SEM. Fig. S19 (a) and (b) show ion defects exist inside the crystal matrix of the particle, and EDS analysis demonstrates the particle has the Fe/O atom ratio much higher than 3:4. Therefore, the defects were caused by O²⁻ ions diffusion from inside toward outside.

The proportional relationship between $i(i)$ and v at low scan rate verified that the reduction was the surface reaction, which meant O²⁻ ions diffusion was relatively fast, and the diffusion distance was very short. With increasing scan rate, the change of the relationship between $i(i)$ and v proves O²⁻ diffusion rate played a more and more important role in the whole reaction rate, and both O²⁻ ion diffusion and the surface reaction controlled the whole reaction rate at moderate scan rate. O²⁻ ion diffusion became the rate-limiting step eventually at high scan rate. The reduced

iron ions at potential of peak (i) must be close to the surface of Fe_3O_4 particles, and the reduced iron ions at potential of peak (ii) must be close to inner center of the particles. The speculation was consistent with not only the relationship that the current density of peak ii was always proportional to square root of the scan rate in a wide range, but also the peak height ratio of i / ii , which increased apparently from 0.2 mV/s to 200 mV/s. The height of peak ii decreased relatively with increased scan rate, because O^{2-} ions, which were from the center of the particle for peak ii , needed to diffuse longer distance than those O^{2-} ions for peak i .

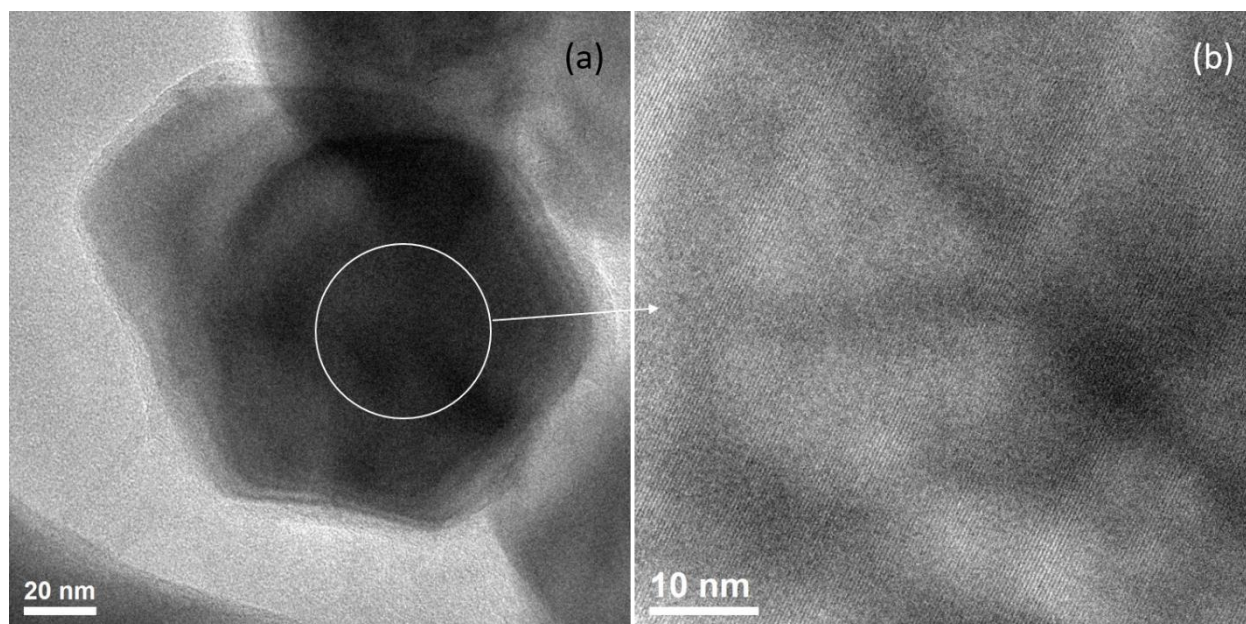


Fig. S19. The Fe_3O_4 particle scanned to -1.132 V (vs. Hg/HgO). (a) TEM analysis of the whole particle; (b) HR-TEM analysis of the same particle with the defects inside the crystal matrix.

Table S6. The calculated peak current density in the CV profiles of Fe_3O_4 (20 nm) ink electrode with different scan rate.

Scan rate / $\text{mV} \cdot \text{s}^{-1}$	Calculated current density of peak i / $\text{mA} \cdot \text{cm}^{-2}$	Calculated current density of peak ii / $\text{mA} \cdot \text{cm}^{-2}$
0.2	-0.021	-0.316
0.5	-0.053	-0.515
1	-0.101	-0.304
2	-0.185	-0.554
6	-0.523	-0.870
10	-0.761	-1.327
20	-1.321	-1.753
50	-2.850	-3.221
100	-4.661	-4.943
200	-7.377	-6.617

10. SEM characterization of γ -Fe₂O₃ particle and CV test of γ -Fe₂O₃ ink electrodes

The morphology of γ -Fe₂O₃ particle on glass carbon was analyzed by SEM, as shown in Fig. S20, and γ -Fe₂O₃ ink electrodes were prepared by using the particle. Each electrode was just tested once at a scan rate, and their CV profiles were shown in Fig. S21. Three cathodic peaks

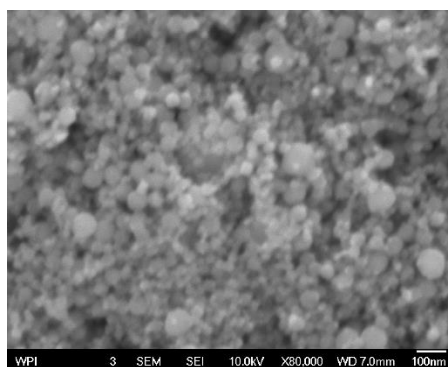


Fig. S20. The morphology of γ -Fe₂O₃ particle.

appear in the CV profile, which are marked as peak i, ii and iii in the figure. The peak current density of peak i, ii and iii was proportional to the square root of scan rate, as shown in Fig. S22, and the relationship proved that O²⁻ ions diffusion inside γ -Fe₂O₃ particles was the rate-

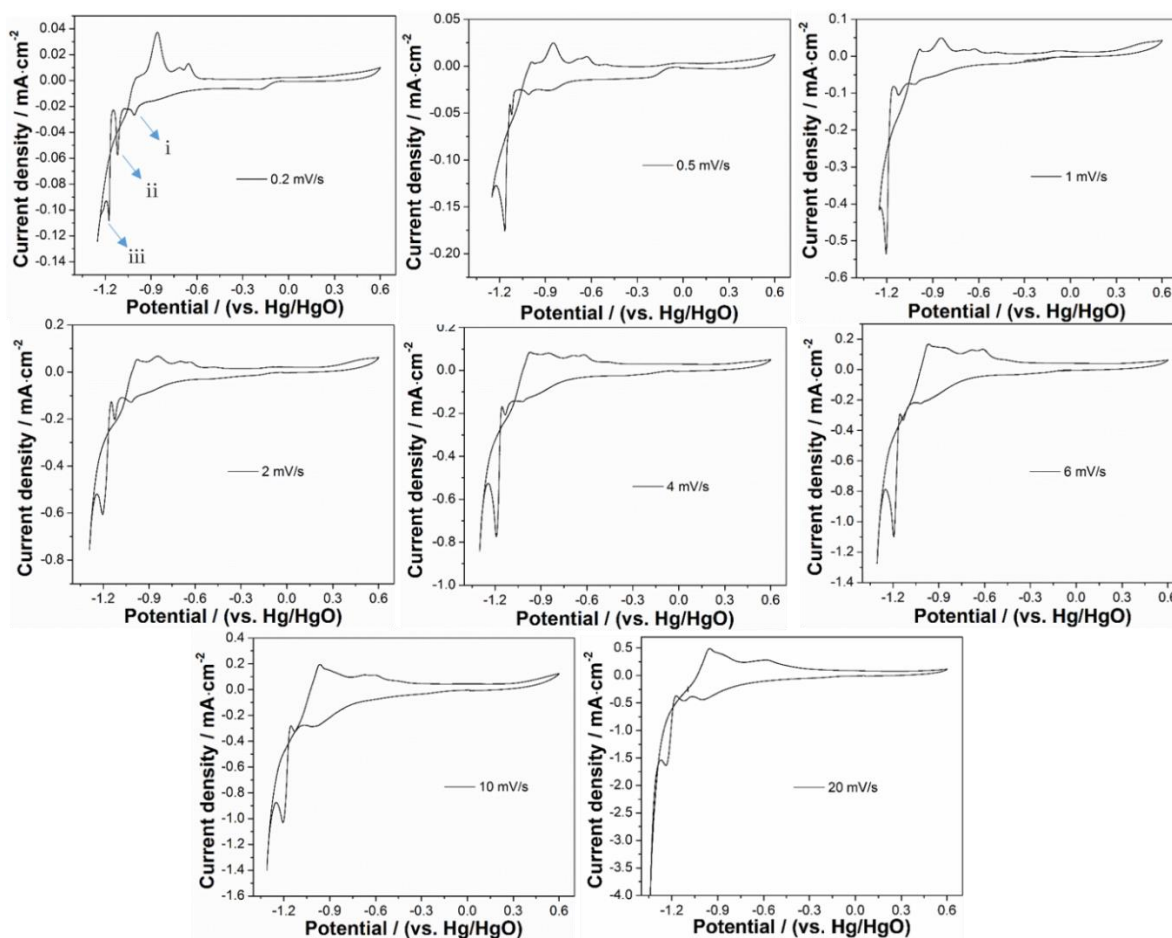


Fig. S21. The CV profiles of the γ -Fe₂O₃ (40nm) ink electrodes in 20 wt% KOH solution with a series of scan rates from 0.2 mV/s to 100 mV/s.

limiting step.

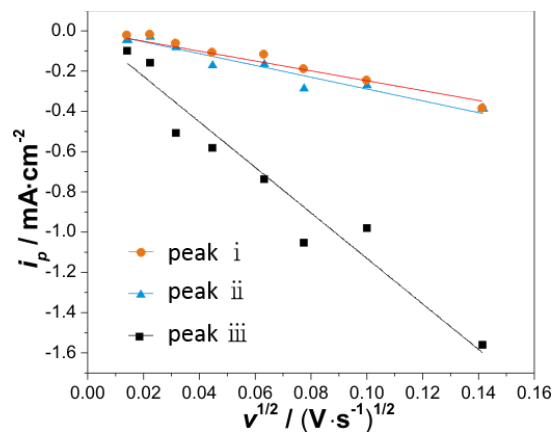


Fig. S22. The relationship between current density of peak i , ii and iii and the scan rate. The current density of all the peaks was proportional to square root of the scan rate.

Table S7. The calculated peak current density in the CV profiles of γ -Fe₂O₃ (40nm) ink electrode with different scan rates.

Scan rate / mV · s ⁻¹	Calculated current density of peak i / mA·cm ²	Calculated current density of peak ii / mA·cm ²	Calculated current density of peak iii / mA·cm ²
0.2	-0.019	-0.049	-0.100
0.5	-0.015	-0.035	-0.159
1	-0.060	-0.087	-0.508
2	-0.105	-0.176	-0.582
4	-0.115	-0.171	-0.737
6	-0.186	-0.291	-1.053
10	-0.243	-0.276	-0.980
20	-0.382	-0.390	-1.560

Note 1

Estimation of O²⁻ diffusion coefficient (D)

O²⁻ diffusion coefficient can be roughly estimated from equation (2) in the manuscript. For most of electrochemical reactions, α in equation (3) is usually around 0.5, and other α values are also applied to estimate D value. However, the challenge is to estimate the electrode area. For planar electrode in solution, A is the apparent area of electrode. In this work, oxide particles pile on glass carbon in the way of layer by layer. Because the electrical conductivity of oxides is usually very low, and the contact resistance between two particles is large, the initial electrochemical reaction interface is the contact points between oxide particles and glass carbon. During the reduction reaction process, O²⁻ ions diffuse outward from the crystal matrix of the particles, and react with electrolyte. Therefore, the real surface area of the particles contacting with glass carbon can be considered as the surface area of electrode (A). The number of the particles in each layer is estimated on the base of the assumption as follows: (1) each particle has the same diameter; (2) all these particles, which directly contact with glass carbon, are tangent with each other, as shown in Fig. S23. The centers of three tangential circles are connected together, and a regular triangle

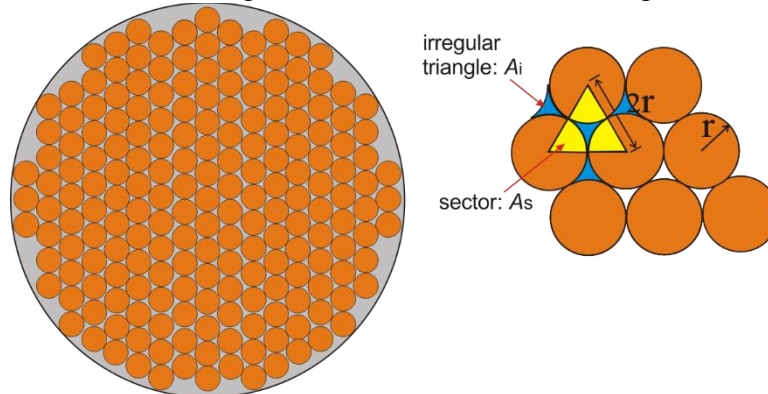


Fig. S23: The arrangement of particles on the surface of glass carbon. The irregular triangle (blue color) is surrounded by three particles.

forms. The radius of each circle is r , thus the side length of the regular triangle is $2r$. The area of the regular triangle (A_r) is $\sqrt{3}r^2$. Three tangential circles surround an irregular triangle (A_i), and the areas of the regular triangle is equal to the total area of three sectors and one irregular triangle, as shown in Fig. S 23.

$$A_r = A_i + 3A_s \quad (S1)$$

In the equation S1, A_s is the area of the sector, and the value is $\pi r^2/6$. A_i is area of the irregular triangle, which is $(\sqrt{3} - \pi/2) r^2$. The area of glass carbon, which is covered by tangential particles, includes the area of the circles and the irregular triangles. Three tangential circles introduce four irregular triangles, and then one additional tangential circle helps to introduce two more irregular triangles. Assuming that the number of oxide particles, which directly contact with glass carbon, is n , therefore the total number of irregular triangles is $[4 + (n-3)*2]$, and the total coverage area by these particles is $[4 + (n-3)*2]* (\sqrt{3} - \pi/2) r^2 + n*\pi r^2$, which should be almost equal to the area of glass carbon: $\pi*(2.5*10^{-3})^2 \text{ m}^2$.

$$[4 + (n-3)*2]* (\sqrt{3} - \pi/2) r^2 + n*\pi r^2 = \pi*(2.5*10^{-3})^2 \quad (S2)$$

In the equation S2, if $r = 20*10^{-9} \text{ m}$, then n is $1.417*10^{10}$. The surface area of electrode (A) is the surface area of particles contacting with glass carbon directly, and the value can be calculated as equation S3 shown:

$$A = n * 4\pi r^2 \quad (S3)$$

A is about 0.71 cm², and it is applied in equation (2) to estimate D. The surface area of electrode is estimated with other particle size, and results demonstrate the value of the surface area of electrode is close to 0.712 cm², no matter how large the particle size is. (If particle size is about 30 nm, the number of particles, which contact with glass carbon, is about 2.519*10¹⁰, and A value is still 0.712 cm². If particle size is about 200 nm, the number of particles, which contact with glass carbon, is about 5.668*10⁸, and A is 0.712 cm².) The molarity of O²⁻ ion inside different oxides was calculated based on the density of oxides, as shown in Table S8. After the slope of the fitting line in the graph of *i_p* and *v*^{1/2} linear relationship is determined, the diffusion coefficient at different peak potential can be calculated on the base of equation (2), and the value is shown in Table S9.

Table S8. The density, molarity of different oxides, and O²⁻ ion molarity in oxides.

catalogue	density (g/cm ³)	Molarity of oxide (mol/ml)	molarity of O ²⁻ (mol/ml)
α-Fe ₂ O ₃	5.24	3.28*10 ⁻²	9.83*10 ⁻²
γ-Fe ₂ O ₃	5.24	3.28*10 ⁻²	9.83*10 ⁻²
Fe ₃ O ₄	5.18	2.23*10 ⁻²	8.93*10 ⁻²
Bi ₂ O ₃	8.9	1.91*10 ⁻²	5.73*10 ⁻²
CuO	6.4	8.05*10 ⁻²	8.05*10 ⁻²

Table S9. O²⁻ diffusion coefficient inside different oxides, unit: cm²/s.

transfer coefficient	α-Fe ₂ O ₃ (40 nm)	α-Fe ₂ O ₃ (200 nm)	γ-Fe ₂ O ₃ (30 nm)			Fe ₃ O ₄ (20nm)	2nd reduction peak	Bi ₂ O ₃ (30 nm)	CuO (30 nm)
	1st reduction peak	1st reduction peak	1st reduction peak	2nd reduction peak	3st reduction peak	1st reduction peak		1st reduction peak	1st reduction peak
0.5	4.86*10 ⁻¹³	4.48*10 ⁻¹³	3.84*10 ⁻¹⁴	7.34*10 ⁻¹⁴	1.65*10 ⁻¹²	5.87*10 ⁻¹²	2.35*10 ⁻¹²	3.04*10 ⁻⁹	3.34*10 ⁻¹⁰
0.2	1.21*10 ⁻¹²	1.12*10 ⁻¹³	9.61*10 ⁻¹⁴	1.83*10 ⁻¹³	4.11*10 ⁻¹²	1.47*10 ⁻¹²	5.90*10 ⁻¹²	7.60*10 ⁻⁹	8.34*10 ⁻¹⁰
0.3	8.10*10 ⁻¹³	7.47*10 ⁻¹³	6.41*10 ⁻¹⁴	1.22*10 ⁻¹³	2.74*10 ⁻¹²	9.78*10 ⁻¹²	3.91*10 ⁻¹²	5.07*10 ⁻⁹	5.56*10 ⁻¹⁰
0.7	3.47*10 ⁻¹³	3.20*10 ⁻¹³	2.75*10 ⁻¹⁴	5.24*10 ⁻¹⁴	1.18*10 ⁻¹²	4.19*10 ⁻¹²	1.68*10 ⁻¹²	2.17*10 ⁻⁹	2.38*10 ⁻¹⁰
0.8	3.04*10 ⁻¹³	2.80*10 ⁻¹³	2.40*10 ⁻¹⁴	4.59*10 ⁻¹⁴	1.03*10 ⁻¹²	3.67*10 ⁻¹²	1.47*10 ⁻¹²	1.90*10 ⁻⁹	2.08*10 ⁻¹⁰

After getting the diffusion coefficient, O²⁻ diffusion distance can be calculated according to equation S4:

$$\delta = (Dot)^{1/2} \quad (S4)$$

t in the equation is the time that species spend for diffusion. The ratio between the diffusion distance and thickness of oxide layers on the surface of glass carbon indicates the weight percentage of oxide involving in reduction reaction based on the calculation. The actual amount of oxide involving in reduction can be obtained by integrating cathodic current of CV profile. The cathodic curve of the CV profile of the ink electrode was integrated, and the integration value was divided by scan rate, then the charge from both oxide reduction and electric double layer was obtained. The CV test was carried out for glass carbon electrode with the same electrolyte and scan rate, and the integration of the cathodic curve of the CV profile corresponded to the charge from electric double layer. Therefore, the charge from oxide reduction can be obtained by subtracting the charge of electric double layer from the total charge. Since the total weight of oxide on glass carbon is 50 μg, the actual weight percentage of oxide involving in reduction can be obtained. By comparing the calculated value and experimental value, the accuracy of calculated diffusion coefficient can be examined.

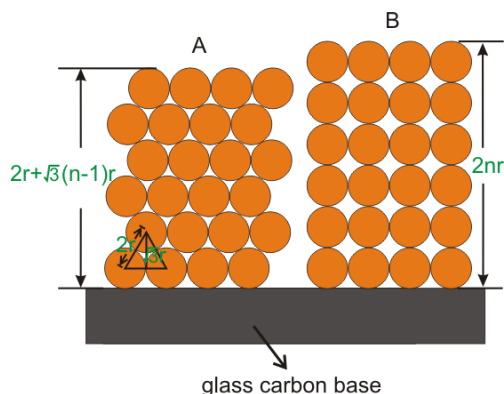


Fig. S24. The maximum and minimum height of oxide particles piling on glass carbon. A. the piling pattern with minimum thickness; B. the piling pattern with maximum thickness.

The total thickness of oxide layers on the surface of glass carbon can also be estimated. Take the particle with 40 nm diameter for example. For a monolayer, the number of the particles on the surface of glass carbon (5 mm diameter) is 1.417×10^{10} , and the total weight of particles is 50 μg . Therefore, $1.417 \times 10^{10} \times 4\pi(r)^3/3 \times m \times 6.4 \text{ g/cm}^3 = 50 \times 10^{-6} \text{ g}$. (m is the number of layers of oxide particles on glass carbon). m is calculated to be 16.45. Fig. S24 shows two ideal ways, which have the maximum and minimum thickness of the oxide layer piling on the surface of glass carbon evenly. Fig. S24 A shows the minimum thickness of the layers is $2r + \sqrt{3}(m-1)r$, and B shows the maximum thickness of the layers is $2mr$. r is the radius of particles. If the distribution of the particles is even, the thickness of the particle (40 nm diameter) layers is between 575.2 nm and 658 nm. However, oxide particles distribution may not be even on the surface of glass carbon in reality. Some particles may accumulate on one spot making the thickness larger than 658 nm, and other spots may have less than 575.2 nm thick, causing deviation between the calculation and experimental values.

In the CV profile of γ -Fe₂O₃ ink electrode, at a scan rate of 0.2 mV/s, the base width of the reduction peak is about 0.624 V, and it takes 3120 s to scan the width of 0.624 V. According to equation S4, O²⁻ ions can diffuse 55.9 nm during this time. In the same way, the distance of O²⁻ diffusion with other scan rates is calculated, as shown in Table S10. Theoretically, the thickness of γ -Fe₂O₃ layer on glass carbon is between 575.2 nm and 658 nm. The ratio between O²⁻ diffusion distance and the thickness of γ -Fe₂O₃ layer is the weight percentage of γ -Fe₂O₃ involving in reduction according to calculation. Table S10 shows O²⁻ diffusion distance, weight percentage of γ -Fe₂O₃ involving in reduction according to calculation and experiments. In the table, the weight percentage of γ -Fe₂O₃ involving in reduction is calculated based on 620 nm thick γ -Fe₂O₃ on glass carbon. and the value has no significant change even if the thickness changes from 575.2 nm to 658 nm. Table S10 shows that the calculation value is closed to experimental one, thus verifying that O²⁻ diffusion coefficient in γ -Fe₂O₃ is reasonable.

Table S10 Comparison between the calculated and actual weight percentage of γ -Fe₂O₃ involved in electrochemical reduction.

Scan rate	Base width of the reduction peak / V	Peak time / sec*	O ²⁻ diffusion distance / nm	Weight percentage of γ -Fe ₂ O ₃ involved in	Weight percentage of γ -Fe ₂ O ₃ involved in electroreduction

				electroreduction (from calculation)	(from experiment)
0.2 mV/s	0.624	3120	55.9	0.090	0.055
0.5 mV/s	0.538	1076	32.8	0.053	0.044
1 mV/s	0.583	583	24.1	0.039	0.037
2 mV/s	0.574	287	16.9	0.027	0.029
4 mV/s	0.565	141.3	11.9	0.019	0.017
6 mV/s	0.6	100	10	0.016	0.018
10 mV/s	0.591	59.1	7.7	0.012	0.013
20 mV/s	0.7	35	5.9	0.0095	0.0086

*“Peak time” means time consumed for scanning, when electrode potential was scanned from right side of the peak base to left side of the peak.

With 40 nm of the particle size, O²⁻ diffusion coefficient of CuO is also examined in the same way as γ -Fe₂O₃ did, and Table S10 shows the weight percentage of CuO involving in reduction by calculation and experiment. However, the fitting is not as good as γ -Fe₂O₃'s. The irregular shape of CuO particles, and their uneven distribution, which is shown in Fig. S10, are the main reasons of the fair consistency. However, the calculated and experimental data indeed show some consistency. When the scan rate is lower than 40 mV/s, O²⁻ diffusion distance is larger than 570 nm according to calculation, and this value demonstrates that diffusion distance is near or larger than the theoretical thickness of CuO particle layers and most of CuO particles can involve in reduction. Therefore the quantity of CuO particles involved in reduction should be constant when scan rate is lower than 40 mV/s. Both calculation and experiment data indeed verify this point in Table S11. When scan rate is 100 mV/s, O²⁻ diffusion distance is 240 nm according to the calculation, which is about one third of the theoretical thickness of CuO particle layers. Experimental data also verifies this point.

Table S11 Comparison of the calculated and experimental weight percentage of CuO involved in electrochemical reduction.

Scan rate	Width of the reduction peak base / V	Peak time sec*	O ²⁻ diffusion distance / nm	Weight percentage of CuO involved in electroreduction (from calculation)	Weight percentage of CuO involved in electroreduction (from experiment)
1 mV/s	0.4	400	2000	1	0.835
2 mV/s	0.53	263	1600	1	0.6515
6 mV/s	0.59	98	1000	1	0.705
10 mV/s	0.63	63	800	1	0.675
20 mV/s	0.63	32	570	0.919	0.687
40 mV/s	0.63	16	400	0.645	0.431
100 mV/s	0.6	6	240	0.387	0.309

*“Peak time” means time consumed for scanning, when electrode potential was scanned from right side of the peak base to left side of the peak.